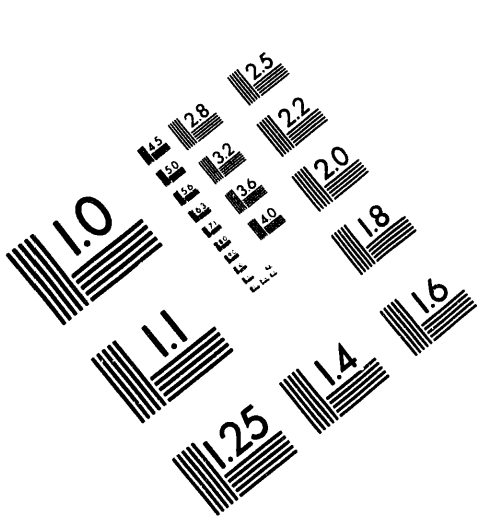

Association for Information and Image Management
1100 Wayne Avenue, Suite 1100
Silver Spring, Maryland 20910
301/587-8202

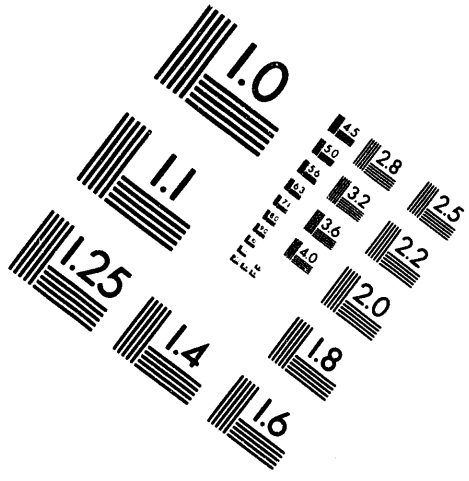

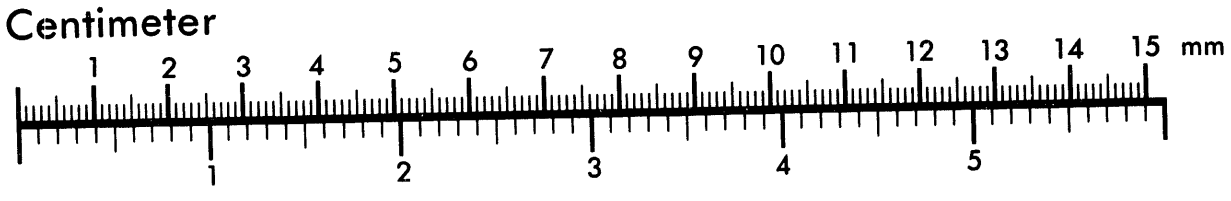

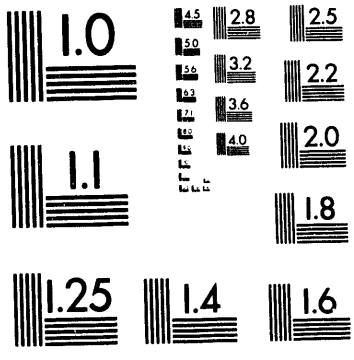

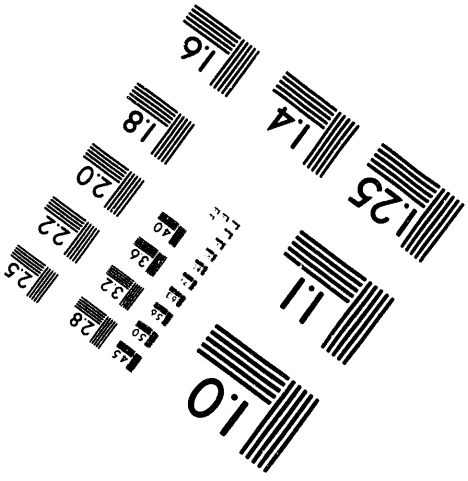

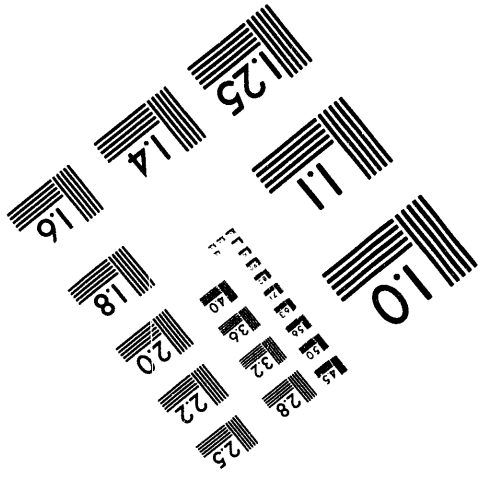

1 of 1

Conf-940892--2

LA-UR- 94-1357

Title: RESERVOIR MICROSEISMICITY AT THE EKOFISK OIL FIELD

Author(s):
J. T. Rutledge
T. D. Fairbanks
J. N. Albright
R. R. Boade
J. Dangerfield
G. H. Landa

Submitted to: EUROCK '94 Rock Mechanics in Petroleum Engineering
A Joint SPE/ISRM Meeting
Delft University of Technology
The Netherlands
August 29 - September 1, 1994

Los Alamos
NATIONAL LABORATORY

Form No. 836 R5
ST 2629 10/91

LA-UR- 94-1357

RESERVOIR MICROSEISMICITY AT THE EKOFISK OIL FIELD

James T. Rutledge, Nambe Geophysical, Inc., Santa Fe, NM, USA
Thomas D. Fairbanks, Nambe Geophysical, Inc., Santa Fe, NM, USA
James N. Albright, Los Alamos National Laboratory, Los Alamos, NM, USA
Rodney R. Boade, Phillips Petroleum Company, Bartlesville, OK, USA
John Dangerfield, Phillips Petroleum Company Norway, Tananger, Norway
Geir H. Landa, Phillips Petroleum Company Norway, Tananger, Norway

Abstract

A triaxial, downhole geophone was deployed within the Ekofisk oil reservoir for monitoring ambient microseismicity as a test to determine if microearthquake signals generated from discrete shear failure of the reservoir rock could be detected. The results of the test were positive. During 104 hours of monitoring, 572 discrete events were recorded which have been identified as shear-failure microearthquakes. Reservoir microseismicity was detected at large distances (1000 m) from the monitor borehole and at rates (> 5 events per hour) which may allow practical characterization of the reservoir rock and overburden deformation induced by reservoir pressure changes.

La microséismicité du réservoir dans le gisement pétrolifère d'Ekofisk

Sommaire

Un géophone triaxial a été déployé dans un sondage dans la roche réservoir de pétrole Ekofisk pour surveiller la microséismicité ambiante. Le but de cet essai a été de déterminer si la détection des signaux de microséismes produits par les ruptures de cisaillement distincts est possible. Les résultats de l'essai sont positives. Pendant 104 heures de surveillance, 572 microséismes distincts de rupture de cisaillement ont été enregistrés. La microséismicité de la roche réservoir a été détectée très loin (1000 m) du sondage en surveillance. Les fréquences des événements (>5 par heure) peuvent permettre la caractérisation de la roche réservoir et de la déformation des morts-terrains produite par les changements de pression dans la roche réservoir.

Reservoir Mikroseismizität im Ekofisk Ölfeld

Abstract

Ein triachsiales, Bohrloch-Geophon zur Überwachung der Hintergrund-Seismizität wurde im Ekofisk Ölfeld eingesetzt, um zu testen, ob Mikrobeben von diskreten shear-failures im Reservoir aufgezeichnet werden können. Die Testresultate waren positiv. Während eines Überwachungszeitraumes von 104 Stunden konnten 572 diskrete Beben aufgenommen werden, die als shear-failure Mikrobeben identifiziert wurden. Mikroseismizität im Reservoir wurde auf grosse Distanzen (>1000 m) vom Bohrloch und mit grosser Häufigkeit (>5 Beben pro Stunde) festgestellt. Dies könnte zur praktischen Nutzung dieser Ereignisse für eine Charakterisierung des Reservoirgesteins sowie der durch Druckänderung im Reservoir hervorgerufenen Deformationen genutzt werden.

Introduction

The Ekofisk field, located in the Norwegian sector of the North Sea, produces from a chalk reservoir at approximately 3 km depth below the seafloor. The reservoir forms an elliptical dome with an areal coverage of 49 km^2 and a production interval approximately 305 m thick. Two fractured chalk formations make up the reservoir, the Ekofisk and Tor formations of Danian and Maastrichtian age, respectively. Average porosities are 32% in the Ekofisk formation and 30 percent in the Tor formation.[1] Small pore throats result in a low matrix permeability of about 1 md.[2] An extensive natural fracture system primarily controls the reservoir permeability and oil production. Fracture permeabilities as high as 150 md have been suggested from well test data.[3]

In November, 1984 evidence of seafloor subsidence was discovered at Ekofisk as a results of reservoir compaction induced by fluid withdrawal. Since then efforts have been made to numerically simulate reservoir compaction and subsidence, among other technical programs, for predicting subsidence. These studies have been motivated by a need to anticipate problems in managing the

reservoir and a need to identify required modifications to offshore facilities. The primary mechanism used in the early simulation models was pore collapse of the reservoir rock due to effective stress loading accompanying fluid withdrawal.[4] Reservoir pressure estimates were used as the basic input data for predicting subsidence and compaction. Pressure decline rates slowed in the late 1980's due to reduced production rates and water injection operations. The observed subsidence since 1985, however, was greater than the pore-collapse models predicted suggesting that pore-collapse was not the only mechanism active in the Ekofisk reservoir. A more recent compaction/subsidence model incorporating shear-induced compaction in addition to pore collapse has improved the agreement between observed and calculated subsidence magnitudes and rates.[5]

The shear-induced compaction model is supported by the observations of highly anisotropic stress loading accompanying reservoir pressure decline. Laboratory stress/strain measurements and in-situ stress measurements indicate that the deviatoric stress growth caused by fluid extraction at Ekofisk should result in Mohr-Coulomb shear failure of the reservoir rock and/or slippage along existing fractures.[6] The effective stress changes accompanying local pressure recovery during waterflooding further induces shear failure.[7] If the induced shear failure occurs discretely, the phenomenon could be observed directly as microearthquakes. This paper presents the results of a test in which a borehole seismometer (geophone) was placed within the Ekofisk reservoir to determine if such microearthquake signals could be detected. Downhole microseismic monitoring offers the advantage of enabling reservoir fracture mechanic characterization at large distances from a borehole.[8] Potentially, microseismic data could provide measurements of fracture/displacement dimensions, stress orientations, faulting mechanism and individual fracture locations along which displacement is induced.

Deployment and Data Acquisition

The geophone package used was equipped with 3 orthogonal, 8 Hz geophone components. Extension of a mechanical arm couples the package to the borehole wall. The analog geophone output is amplified 60 dB downhole before transmission uphole. At the surface the data signals are anti-alias filtered and further amplified before input to a digital, PC-based, data acquisition system. The PC stores discrete signals captured by an algorithm which triggers on signal levels of a specified amplitude over a continuously-measured background level. The digital sample interval was 0.2 ms.

The geophone tool was deployed in well C-11 during the third week of February, 1993. Well C-11 is a non-producing, vertical well dedicated for periodic compaction strain measurements through the reservoir production interval.[9] The reservoir producing interval is intersected from approximately 2930 to 3135 m. The well liner is not perforated. Accumulation of wellhead pressure during shut-in periods however, indicates that fluids leak into the borehole. Without wellhead pressure containment, high noise levels were observed on the geophone output at all depths occupied (ranging from 1830 to 3290 m depth). Continuous high noise conditions were predominant on the 2 horizontal geophone components. In addition, discrete "noise bursts" were observed every few seconds on all 3 components. The noise response may have been due to gas bubbles rising past the tool and/or gas bubbling into the wellbore acting as a source of tube-wave energy (acoustic energy guided along the borehole-wall/fluid interface).

The wellhead was pressurized to 7 MPa (1000 psi) by injecting natural gas. This reduced the background borehole noise observed predominantly on the horizontal components by approximately 20dB and reduced the frequency of noise bursts to about 1 event every 5 minutes. Under the containing wellhead pressure, the reduced noise conditions did not significantly vary with depth. For the long-term monitoring the geophone was stationed at 2985 m depth, within the Ekofisk Formation where the measured reservoir compaction is greatest.

The geophone package and data acquisition system operated almost continuously for a 106-day period (February 18 to June 4, 1993). However, noise conditions in well C-11 deteriorated on February 24 and never stabilized for the remainder of the experiment. For reasons that are unknown, the wellhead pressure could not be maintained at 7 MPa (1000 psi). Subsequent attempts to lower noise levels by repressurizing and raising the fluid level were not successful. During the first 6 days of monitoring, there was a cumulative 104-hour period of monitoring coverage with low, stable noise levels. The data presented in this paper were collected during this 104-hour period.

Data Analysis

During the 104-hour monitoring period there were approximately 1800 triggered signals recorded on the PC data acquisition system. Of these, 572 events in which both a P- and S-wave phase could be identified have been selected as probable microearthquake events (e.g. Figure 1). This corresponds to a detection rate exceeding 5 events per hour. Due to the nature of the source, microearthquakes resulting from shear failure, like tectonic earthquakes, have more energy in the S-wave phase. With detection at a single station, we can only determine source-receiver distances for the 2 phase events. Many other triggered events may

have also been microearthquake signals but only showed a single, clear phase. The majority of triggered events were rejected as possible microearthquake signals. Some possible causes of the "noise" events are discussed below.

The source-receiver distance can be computed from the S- P-wave arrival time difference for those events in which both phases can be identified provided the P- and S-wave velocities (Vp and Vs, respectively) are known. An average Vp of 2750 m/sec was used, determined from the C-11 sonic log, and a Vp/Vs ratio of 1.7 was assumed. Figure 2 shows the distance distribution for the 572 events in which both P- and S-wave phases were identified. Events were detected up to 1000 m from the geophone package. The majority of events detected occurred within 400 m of the geophone package.

Spectra

Figure 3 shows an example of the S-wave displacement amplitude spectra of an event occurring approximately 425 m from the geophone package. The shape of the spectra is characteristic of shear-slip displacement signals.[10] The spectra consist of a low-frequency spectral amplitude response (flat portion), a corner frequency and a linear roll-off beyond the corner frequency with a slope of approximately -3. The roll-off can be described as ω^{-3}, where ω is the angular frequency. For shear-slip earthquakes and microearthquakes, the spectra roll-off above the corner typically ranges from ω^{-2} to ω^{-3}. Corner frequencies ranged from about 80 to 250 Hz.

Seismic Recurrence

Quantifying the recurrence rate of the microseismicity at Ekofisk may be useful for predicting the time necessary to record a given number of events exceeding some magnitude from a given location within the field. Graphically the recurrence can be represented by a plot of the cumulative number of events N greater than some magnitude m. The slope of such a plot has been observed to be constant over some magnitude range and is referred to as the b-value[11], where

$$\log N = a - bm.$$

A b-value of 0.7 was computed over a relative earthquake magnitude range of $3\frac{1}{2}$ (Figure 4). The relative magnitude scale is a pseudo-magnitude scale computed similar to Aki[12], where magnitude is taken as the log of the amplitude measured from the coda of each seismic event at a fixed lapse time after the event origin time. Reliable measurements were made on 221 of the 572 events in which P- and S-phases were identified. In addition to giving the rate of increase of the number of microearthquakes with decreasing magnitude, Figure 4 also flattens out at lower magnitudes indicating a magnitude threshold at which no more microearthquakes were detected.

The b-value also gives a measure of the relative distribution of seismic energy released with event size. Values equal to or less than 1, such as measured for the first 104 hours of monitoring, generally imply that most of the strain energy release is dominated by the smaller number of large events.[13] This in turn implies that the total strain energy release can be estimated from such a data set because smaller events below the threshold of detection are not making a significant contribution to the total energy release. Longer term monitoring over a larger area of the field would be required to characterize the microseismic recurrence of the reservoir and overburden rock, in general.

Empirical scaling relationships between seismic coda durations and local magnitudes have been determined for several regions of the world.[11] Coda duration is the time from the P-wave onset to the time when the coda amplitude decays to background noise levels. The coda durations at Ekofisk ranged from about 4.0 to 0.05 seconds. There has been a small amount of regional seismicity in the Ekofisk area,[14] but no such scaling relationship to local magnitudes have been determined. Using formulas established in different regions of the western United States would fix the magnitude scale range of Figure 4 from -4 to 0 [11] or -6 to -2 [15] Richter magnitudes.

Mapping Microearthquakes and Selection Criteria

From a single, 3-component geophone receiver, a direction to a seismic source can be determined from the P-wave polarization trajectories. Projecting back along the trajectory by the distance determined from the S- P-wave traveltime difference, gives the microearthquake source location. There is a 180° ambiguity in the trajectories determined from a single geophone packages. The direction to the source could correspond to a compressional first arrival from the indicated direction or a dilational first arrival from the opposite direction. The orientation of linear or planar trends will be identical for both solutions though absolute locations are unknown. Detection at more than one receiver location will resolve the ambiguity.

The geographic orientation of the geophones' horizontal axes can be determined by detecting a seismic source at a known location. An attempt was made to orient the geophone axes using an airgun seismic source suspended beneath the sea surface. The orientation shots did not work because the noise levels in the well had deteriorated to the levels observed with no wellhead pressure. Relative event locations can be displayed with respect to the horizontal geophone axes without the geographic orientation. The resulting map view of locations needs to be rotated by some unknown

angle. Interpretation of the location depths is more meaningful since the vertical geophone orientation is known.

The polarization trajectory is taken as the orientation of the major axis of an ellipsoid fitted to the 3-dimensional seismic particle motion.[16] Three projections of first arrival particle motion are shown in Figure 5 for a 2 msec window of P-wave data. The window width is minimized to avoid any tool resonances and secondary arrivals. Straight raypaths and an average P-wave velocity of 2750 m/sec were used in projecting back to the source locations. Four successive selection criteria were used for determining well constrained event locations. 1) The signal-to-noise ratio of the first motions had to exceed 5.0. 2) The contribution of the principal axis of particle motion to the sum of all 3 axes had to be greater than 0.85. This is a constraint on the linearity of the particle motion. A contribution factor of 1.0 is perfect; spherical particle motion would have a contribution of 0.33. 3) The inclination of the particle motion had to be within ±70°. This third selection criteria was to eliminate any discrete tube-wave arrivals which were mistakenly identified as microearthquakes. The particle motion of a tube-wave arrival will point vertically (inclination = 90°), along the axis of the borehole (e.g. Figure 6). 4) The particle motions of the P- and S-waves first arrival had to be orthogonal, ±20°. In a homogeneous medium, the respective particle motions will be orthogonal. This last selection criteria verifies the S-wave pick. Table 1 shows the number of events that passed each successive test for the 104-hour monitoring period.

Criterion	Number Passed
Acquisition system triggered	1800
P– and S–waves identified	572
1) P–wave signal–to–noise > 5.0	454
2) Particle motion principle axis contribution > 0.85	345
3) Particle motion inclination < ±70°	176
4) P– and S–wave particle motions are orthogonal	72

Table 1. The sequence of selection criteria used in discriminating the microearthquakes with the most reliable locations. Also included are the number of signals recorded by the triggered data acquisition system and the subsequent visual selection of candidate, shear–slip microseismic events.

Selection criteria 1 and 2 eliminate 40 percent of the candidate events from being located. The first arrivals of the data were, in general, very emergent (i.e. not impulsive). The low quality of the first arrivals is probably due to high attenuation of seismic energy within the reservoir rock. High attenuation should be expected in the chalk due to the high porosity (36% in the vicinity of well C-11), the presence of fractures, and low velocities (Vp=2750 m/sec). Nearly 50 percent of the impulsive arrivals that were picked could possibly be tube-wave events. The last selection criterion indicates that only 40 percent of the impulsive, non-tube-wave arrivals have S-wave particle motions that are perpendicular to the P-wave particle motion. Failure to satisfy selection criteria 1, 2 and/or 4 does not imply that the events are not shear-slip microearthquakes, but that the quality of the signals are inadequate for locating the events from a single, 3-component geophone tool. Seventy two events can be mapped with a high degree of confidence.

In addition to the 169 possible "tube-wave" events eliminated by criteria 3, many of the rejected "triggers" also look like tube wave arrivals (vertical particle motion, mono-frequency and long coda). There are many possible ways tube waves could be generated in the monitor well. Fluids or gas pulsing into the borehole could generate discrete tube wave events. The C-11 wellhead pressure has a history of slowing increasing when shut in, which suggests that fluids leak or diffuse into the borehole. As noted above, when the wellhead pressure was not contained, the rate of discrete noise events was much higher than when the well was pressurized.

Tube waves can also be generated from acoustic or seismic energy impinging on any borehole discontinuities such as wellbore terminations, or changes in liner diameter.[17] Microseismic energy impinging on wellbore discontinuities could generate slower (about 1370 m/sec), secondary, tube-wave arrivals along the wellbore. The tube wave (borehole Stoneley wave) is a guided wave and experiences very little energy dissipation along the borehole. Microearthquakes occurring at large vertical distances from the geophone package will not be observed due to body-wave attenuation and scattering. However, if the source is a short radial distance from the monitor well, then body-wave energy impinging on the wellbore could be partially converted to tube-wave energy that would then be detected at the geophone. Seismic energy trapped in stratigraphic wave guides can also efficiently convert to tube waves where the wellbore intersects the wave guide.[18] A vertical array of receivers would be required to determine where tube-wave sources occur in the monitor well and confirm if any seismic body-wave energy is converted to tube-wave energy.

Figure 7 shows the map view of the 72 well-constrained event locations. The axes of the map correspond to the 2 horizontal geophone axes. The geographic orientation of the map is unknown. For each event that could be located, both possible solutions corresponding to the 180 ambiguity are displayed. Circles and squares distinguish the two possible solutions, where the circles represent compressive first arrivals and the squares represent dilational first arrivals. Any possible combination of squares and circles could be the true set of locations provided the "opposite" solutions are

eliminated.

Figure 8 is the depth section projected on to a profile along line A-B of Figure 7. Both possible solutions are again displayed. The majority of the events that passed the selection criteria locate within the reservoir at distances within 200 m of the monitor well. Higher quality signals will be recorded near the geophone because travel paths from source to receiver are shorter, and the signals will have undergone less attenuation and scattering. Only 15 percent of the most highly constrained source locations occur outside the reservoir. If the constraint requiring the P- and S-wave particle motions to be perpendicular is ignored, then approximately 40 percent of the microearthquakes (176 events total) locate above and/or below the reservoir.

Summary

Microseismic, shear-displacement events were detected at rates up to 5 events per hour and at distances of up to 1000 m from the C-11 monitor well over a 104-hour monitoring period. Most events detected occurred within 400 m of the monitor well. The event rate and areal coverage may imply that the ongoing shear deformation induced within and above the reservoir can be practically characterized. Short term monitoring (50 to 100 hours) could reveal major fractures/faults along which displacement occurs up to 1 km from a given borehole. Spectral source characterization could provide statistical dimensions of the shear deformation (e.g. fracture rupture areas, average displacements and stress drops) for a specific volume of reservoir or overburden. Monitoring with a vertical array of geophone receivers would resolve the 180° location ambiguity and would simplify discriminating microseismic events from noise travelling along the borehole. It should also result in a higher proportion of source locations since additional traveltime and particle motion trajectory data will be available.

Acknowledgments

Robert J. Hanold of Los Alamos National Laboratory is gratefully acknowledged for his interest and efforts in initiating this collaborative study between Los Alamos and Phillips Petroleum Company. Special thanks are extended to J. D. Lemons of Phillips Petroleum Company Norway for coordinating the execution of the geophone deployment. The authors acknowledge permission to publish this paper from Phillips Petroleum Company Norway and Co-venturers, including Fina Exploration Norway u.a.s., Norsk Agip A/S, Elf Petroleum Norge AS, Norsk Hydro a.s., Den norske stats oljeselskap a.s., Total Norge A.S, Elf Rex Norge A/S, and Norminol A/S. The opinions expressed in the paper are those of the authors and do not necessarily represent those of the Phillips Norway Group.

References

1. Feazel, C.T., Knight, I.A., and Pekot, L.J.: "Ekofisk Field, Norwegian Sector, North Sea," In: Am. Assoc. Petro. Geol. Atlas of Petroleum Geology, 1990.

2. Thomas, L.K., Dixon, T.N., Evans C.E., and Vienot, M.E.: "Ekofisk Pilot Waterflood," Jour. Petro. Tech. (Feb. 1987) 221-232.

3. Brown, D.: "The Flow of Water and Displacement of Hydrocarbons in Fractured Chalk Reservoirs," In: Fluid Flow in Sedimentary Basins and Aquifers (Goff, J.C., and Williams, B.P., eds), Geological Society of London Special Publication, 34, 201-218, 1987.

4. Boade, R.R., Chin, L.Y., and Siemers, W.T.: "Forecasting of Ekofisk Reservoir Compaction and Subsidence by Numerical Simulation," Jour. Petro. Tech. (July 1989) 723-728.

5. Chin, L., Boade, R.R., Prevost, J.H., and Landa, G.H.: "Numerical Simulation of Shear-induced Compaction in the Ekofisk Reservoir," Int. J. Rock Mech. Min. Sci. & Geomech Abstr. (1993) 30 1193-1200.

6. Teufel, L.W., Rhett, D.W., and Farrell, H.E.: "Effect of Reservoir Depletion and Pore Pressure Drawdown on In Situ Stress and Deformation in the Ekofisk Field, North Sea," In: Proc. 32nd U.S. Symposium on Rock Mechanics, Norman, Oklahoma, July 10-12, 1991.

7. Teufel, L.W., Rhett, D.W.: "Failure of Chalk During Waterflooding of the Ekofisk Field," paper SPE 24911 presented at the 1992 Soc. Petro. Eng. Annual Technical Conference, Washington, D.C., Oct. 4-7.

8. Fehler, M., House, L., and Kaieda, H.: "Seismic monitoring of hydraulic fracturing: Techniques for determining fluid flow paths and state of stress away from a wellbore," In: Proc. 27th U.S. Symposium on Rock Mechanics, Tuscaloosa, Alabama, June 23-25, 1986.

9. Menghini, M.L.: "Compaction Monitoring in the Ekofisk Area Chalk Fields," Jour. Petro. Tech. (July 1989) 735-739.

10. Aki, K., and Richards, P. G.: Quantitative seismology, theory and methods, volume 2, W. H. Freeman and Co., San Francisco (1980).

11. Lee, W. H. K., and Stewart, S. W.: Principles and applications of microearthquake networks: Academic Press, Inc., New York (1981).

12. Aki, K.: "Physical basis for the duration magnitude and recommended practice for coda

magnitude determination," In: Proc. 17th Assembly ESC, Budapest, 1980.

13. Hanks, T.C.; "Small Earthquakes, Tectonic Forces," Science (June 1992) 256 1430-1432.

14. Bungum H., and Selnes P.B.: "Earthquake Loading on the Norwegian Continental Shelf: Summary Report," Norwegian Geotechnical Institute, Oslo, 1988.

15. Sanford, A.R., Olsen, K.H., and Jaksha, L.H.: "Seismicity of the Rio Grande Rift," In: Rio Grande Rift: Tectonics and Magmatism (Rieker, R.E., ed.), American Geophysical Union, Washington, D.C., 1979.

16. Matsumura, S.: "Three-dimensional expression of seismic particle motions by the trajectory ellipsoid and its application to the seismic data observed in the Kanto District, Japan," J. Phys. Earth (1981) 29 221-239.

17. Hardage, B. A.: "An examination of tube wave noise in vertical seismic profiling data," Geophysics (1981) 46 892-903.

18. Albright, J. N., and Johnson, P. A.: "Cross-borehole observations of mode conversion from borehole Stoneley waves to channel waves at a coal layer," Geophys. Prosp. (1990) 38 607-620.

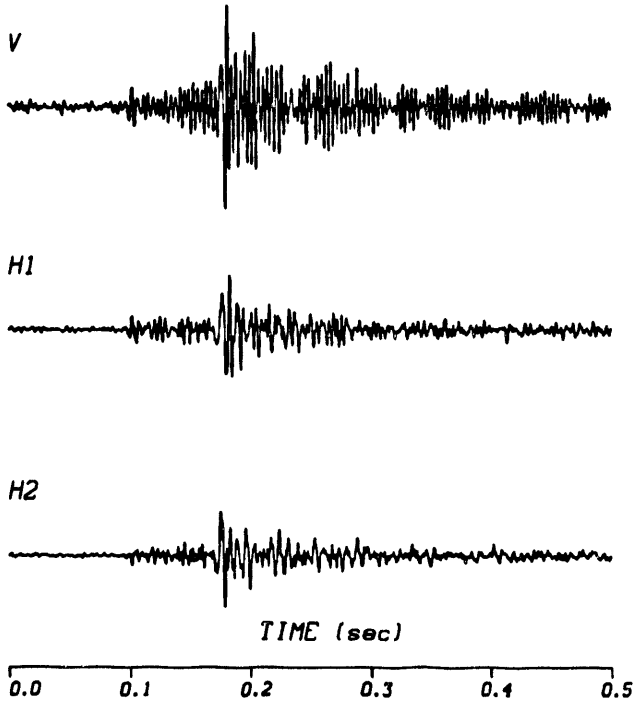

Figure 1. An example of a triggered event that was selected as a potential microearthquake signal. All 3 traces are plotted at the same arbitrary amplitude scale where V is the vertical component and H1 and H2 are the horizontal components. The P-wave arrives at about 0.1 seconds. The S-wave arrives at approximately 0.17 seconds.

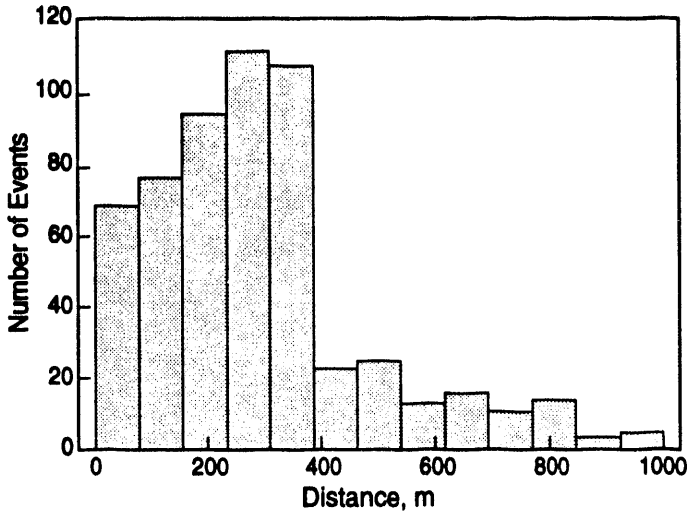

Figure 2. Histogram of the event-distance distribution for the 572 events in which P- and S-wave phases were identified.

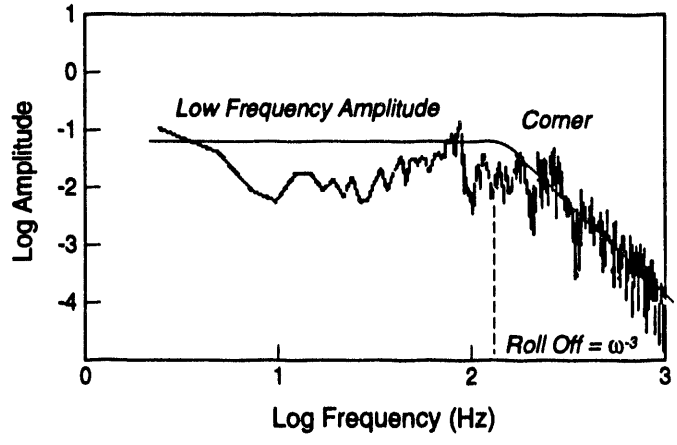

Figure 3. Displacement, S-wave amplitude spectra for a microearthquake occurring approximately 425 m from the geophone. The amplitude scale is in arbitrary units. The observed roll off above the corner frequency is typical for shear-slip events.

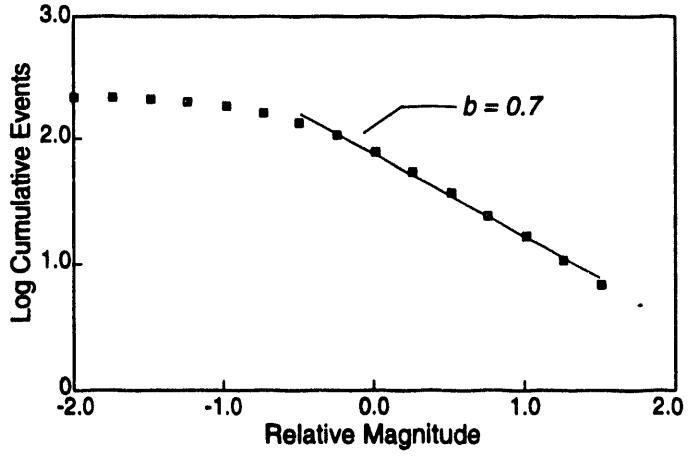

Figure 4. B-value plot for 221 microearthquakes detected from February 18 to 23.

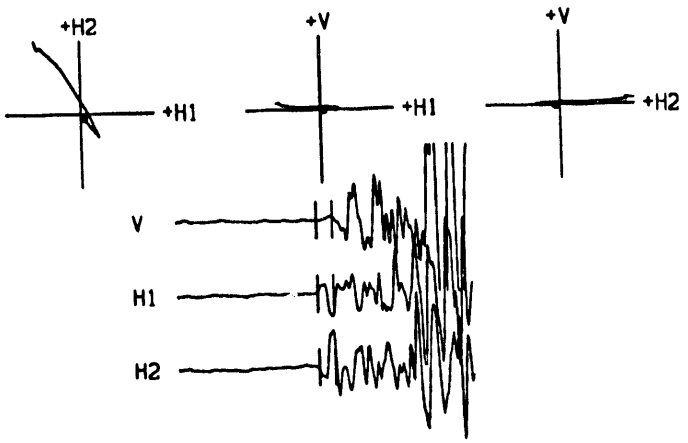

Figure 5. Particle motion projections (above) for the three components of motion detected (below) where V is the vertical component and H1 and H2 are the horizontal components. The vertical bars shown at the P-wave onset for the 3 seismograms mark the window of particle motion displayed above. A two msec window was used.

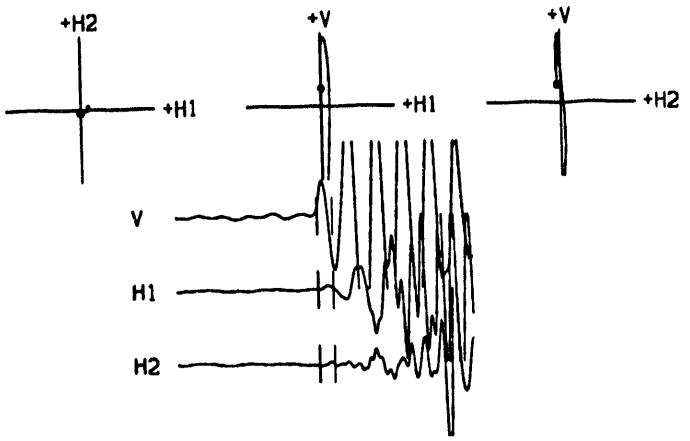

Figure 6. An example of the particle motion for a tube-wave first arrival. Nearly all the energy is detected on the vertical component. The resultant particle motion is, therefore, vertical along the borehole axis.

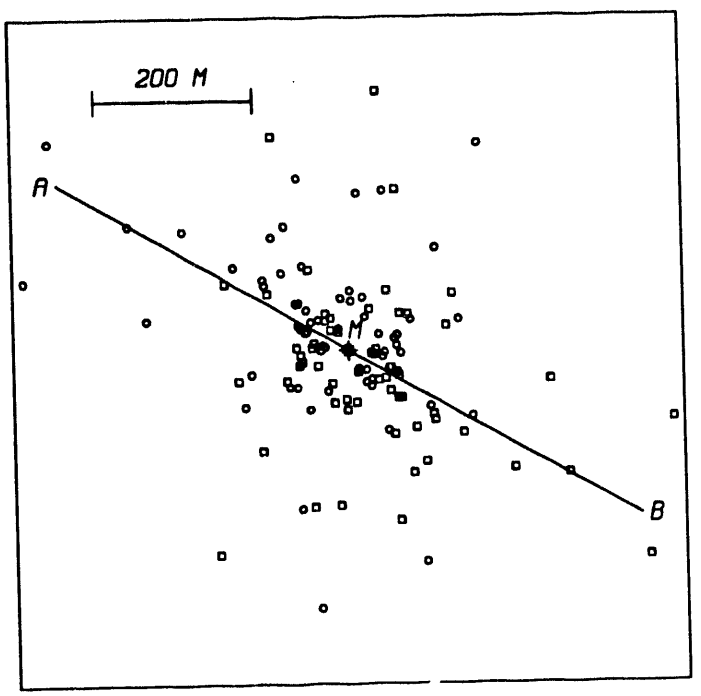

Figure 7. Map view of the 72 well-constrained event locations. The monitor well is marked "M". The map is not oriented; the axes of the map correspond to the geophone horizontal axes (H2 vertical and H1 horizontal). There is a 180° ambiguity in the trajectory determined locations. Therefore, both possible solutions are shown. For each circle there is a corresponding square, located 180° away with respect to the geophone position.

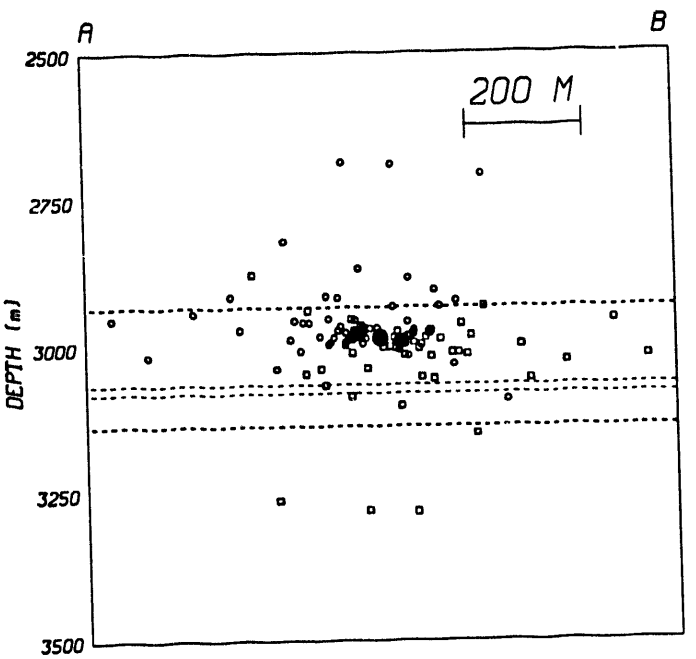

Figure 8. A depth profile of the microearthquake locations projected along line A-B of Figure 7. Both possible solutions for each event are displayed (circles and squares). From top to bottom the dashed lines indicate: 1) top of the Ekofisk formation, 2) top of the tight zone, 3) top of the Tor formation and 4) base of the productive interval of the Tor Formation. The geophone package position is marked with the solid dot, centered along the profile at 2985 m depth.

DATE
FILMED
8/23/94

END